Check for updates

Received: 30 March 2023 | Accepted: 20 April 2024

DOI: 10.1111/arcm.12977

ORIGINAL ARTICLE

Geochemical signature identifying features and archaeological structures in eastern Amazonian Terra Preta sites

Majd Nidal Aboul Hosn[1] | **Bruno Apolo Miranda Figueira**[1] | **Paulo Sérgio Taube Junior**[2] | **José Francisco Berredo Reis da Silva**[3] | **Bráulio Soares Archanjo**[4] | **Kashif Gul**[5] | **Sumeet Malik**[5] | **Marcondes Lima da Costa**[6]

[1]Pós-Graduação em Sociedade Ambiente e Qualidade de Vida, Universidade Federal do Oeste do Pará, Santarém, Pará, Brazil

[2]Instituto de Biodiversidade e Floresta, Universidade Federal do Pará, Santarém, Pará, Brazil

[3]Museu Paraense Emílio Goeldi, Belém, Pará, Brazil

[4]Divisão de Metrologia de Materiais, Instituto Nacional de Metrologia, Qualidade e Tecnologia, Xerém-Duque de Caxias, Rio de Janeiro, Brazil

[5]Department of Environmental Sciences, University of Peshawar, Peshawar, Pakistan

[6]Pos-graduação em Geologia e Geoquímica, Universidade Federal do Pará, Belém, Pará, Brazil

Correspondence
Bruno Apolo Miranda Figueira, Pós-Graduação em Sociedade Ambiente e Qualidade de Vida, Universidade Federal do Oeste do Pará, Santarém, Pará, Brazil.
Email: figueiraufpa@gmail.com

Funding information
Coordination for the Improvement of Higher Education Personnel; National Council for Scientific and Technological Development

Abstract

The present work describes the chemistry and mineralogy of soils such as Terra Preta Arqueológica (TPA) or Terra Preta de Índio (TPI) from the Bitoca I and II sites, located in the Salobo Region (Carajás Mineral Province, Pará-Brazil). The results revealed chemical and mineralogical characteristics that are similar to other TPAs found throughout the Amazon region, such as relatively high levels of Ca (average of 3600 ppm), P (average of 850 ppm), Mn (average of 730 ppm), Zn (average of 55 ppm), and Cu (average of 63 ppm). In soils related to the characteristics of occupation by huts and campfires, the mineralogical composition is represented by quartz, kaolinite, calcite, muscovite, anatase, hematite, goethite, and gibbsite. Amorphous phases have also been identified mainly as calcium phosphates and organic matter (humic and fulvic acids). The analysis of the features/structures described here helped in the identification/verification of areas destined for different activities within the sites.

© 2024 The Authors. Archaeometry © 2024 University of Oxford.

INTRODUCTION

The Amazonian soils modified by prehistoric man are known as Terra Preta (TP), Terra Preta do Índio (TPI), Terra Preta Arqueológica (TPA), Amazonian Dark Earth (ADE) and Archaeoanthrosols (Glaser & Birk, 2012; Kämpf et al., 2009; Silva, 2009). These soils were formed as a result of human occupation, and disposal of organic waste of different nature, which involved the modification of physical, chemical, mineralogical, and microbiological properties (Glaser et al., 2003; Lehmann, Kern, Glaser, & Woods, 2003; Ruivo et al., 2009; Tsai et al., 2009).

The dark color, prolonged permanence of relatively high levels of Ca, Mg, P, Mn, Zn, Cu, and organic C, combined with ceramic fragments and lithic artifacts found in the anthropic horizon, makes TPI a relevant topic in the understanding of studies of Amazonian archaeological sites (Birk et al., 2011; Falcao et al., 2009; Glaser, 2007; Glaser & Birk, 2012; Lehmann, Kern, German, et al., 2003; Schellekens et al., 2017; Schmidt et al., 2014; Taube et al., 2013; Woods et al., 2009). These changes reflect the different uses, times of permanence of old populations, the quantity and quality of discarded organic waste, and the performance of post-occupational (bio) geochemical and pedogenetic processes (Matuk et al., 2020).

Tropical climatic conditions, especially temperature and humidity, impose limitations on the conservation of archaeological remains of an organic nature, mainly. In this aspect, the use of archeometric techniques has been essential in the interpretation of archaeological contexts such as settlement patterns (Athayde & Silva-Lugo, 2018; Posey, 2019), archaeological features and structures (Oonk et al., 2009; Wells et al., 2000; Wilson et al., 2008). Thus, in tropical regions, particularly, anthropic soils are fundamental for the studies of settlement patterns, as they mark the functional areas of old villages that present very different properties in their occupation horizon (Costa et al., 2009; Moutinho et al., 2016).

According to these studies, high concentrations of Ca and P are consistently linked to deposits of organic material that is of animal origin, whereas Cu, Mn, and Zn may be linked to a variety of materials depending on the archaeological context, including mineral pigments, carbonized particles, spaces intended for housing, or even cultivated areas (Falcão & Borges, 2006; Wells et al., 2000; Wilson et al., 2008). A comparatively high concentration of Hg, Fe, Mn, and Cu in the Piedras Negras site in Guatemala suggested regions of ceremonial or handicraft activity. (Wells et al., 2000; Wilson et al., 2008).

According to the potential for linking chemical fingerprints with archaeological settings, it is possible, to a certain extent, understanding the outcome of the cultural and ceremonial diversity among human groups that occupied various levels of social organization in the past. To comprehend certain aspects of ancient Amazonian behavior, this research aims to establish geochemical relationships that identify archaeological features and structures, along with their connection to functional regions resulting from pre-Columbian habitation.

The current research on the geochemical signature of Terra Preta sites in the eastern Amazon adopts a multidisciplinary approach, enhancing our understanding of the region's archaeological and environmental history. The usage of multiple methodologies and a focus on geochemical markers offer a more nuanced perspective on the relationship between ancient human activities and the landscape, fostering a clearer understanding of Amazonian civilizations.

MATERIALS AND METHODS

Location of the study area

Terra Preta de Indio soils, commonly known as Amazonian Dark Earths, are spread out over the majority of the Amazon Basin. Terra preta, which translates to 'black earth' in

14754754, 2024, 6, Downloaded from https://onlinelibrary.wiley.com/doi/10.1111/arcm.12977 by Museu Paraense Emílio Goeldi, Wiley Online Library on [15/01/2025]. See the Terms and Conditions (https://onlinelibrary.wiley.com/terms-and-conditions) on Wiley Online Library for rules of use; OA articles are governed by the applicable Creative Commons License

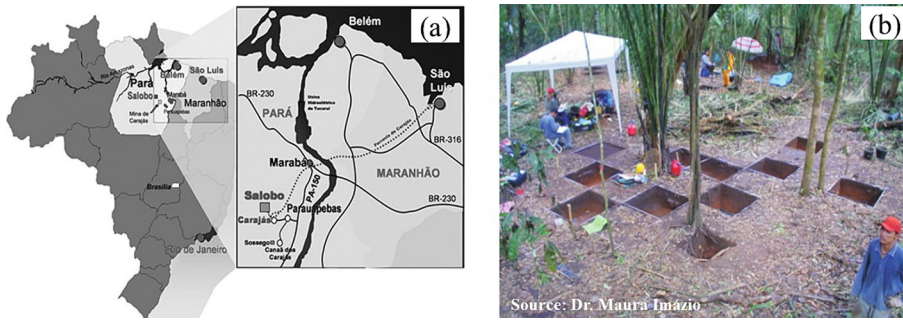

FIGURE 1 (a) Location map of Bitoca I & II sites in Marabá (b) Bitoca II site, with a view of TPA patches (Silveira et al., 2008; Silveira et al., 2009).

Portuguese, stands out from the surrounding soils due to its dark tint. The distinctive characteristics of terra preta, such as their high soil fertility, production capacity, and carbon levels, which have significance for both present sustainable land use and the study of Amazonian civilization development, are what spark interest in them. Although terra preta soils are common throughout the Amazon Basin, little is known about where they might be found. It seems that the central Amazon, between Manaus and Santarem, is where terra preta soils are most prevalent. The Bitoca I and II archaeological sites are in the municipality of Marabá, southeast of the state of Pará, about 600 km from the capital Belém (Figure 1a). These sites were found on the left bank of the Salobo Igarapé, on the low slope, on a terrace with flat parts (forming terraces), and a gentle slope toward the creek. These are large-scale sites measuring approximately 300 m × 300 m, of the open, ceramic, and housing type, with the presence of TPA stains and dark brown soil (Figure 1b). These stains are possibly related to areas of huts, as they present evidence such as marks of holes in pillars and stakes; bonfires; simple ceramics; and decorated in different ways, quartzite and quartz chips, polished axes, and digger (Silveira et al., 2011).

Sampling and preparation—sample nomenclature

The samples used in this work were collected in archaeological salvage fieldwork coordinated by Dr. Maura Silveira and Dr. Dirse Kern. After collection, the samples were coded (Table 1) and stored in plastic bags for further chemical and mineralogical analysis.

Analytical techniques

X-ray diffraction (XRD)

To determine the mineralogical phases present, the soil samples were measured by XRD analysis employing a XPERT PRO MPD diffractometer equipped with a PW 3040/60 (theta–theta), with Cu Ka1 radiation and secondary monochromator, operating at 40 kV/30 mA. The samples were pulverized and mounted into zero background sample holders (obliquely cut silicon crystal). Each diffraction pattern was recorded at a 0.01 2 h step size and count times of 5 s per step. All patterns were evaluated using X'pert Highscore Plus Software from Panalytical.

14754754, 2024, 6, Downloaded from https://onlinelibrary.wiley.com/doi/10.1111/arcm.12977 by Museu Paraense Emílio Goeldi, Wiley Online Library on [15/01/2025]. See the Terms and Conditions (https://onlinelibrary.wiley.com/terms-and-conditions) on Wiley Online Library for rules of use; OA articles are governed by the applicable Creative Commons License

TABLE 1 Origin and nomenclature of the samples in this work.

Archaeological site	Code	Origin
	E7T1SE-7	Bonfire
	E7T1SE-6	Bonfire
	E6T1N-5	Bonfire
	E3SO-1A4	Sediment with ash and burnt clay from bonfire
	E2S3–4	Pile hole sediment, level top
Bitoca 1	E2S13SO-15	Block with fat, central area
	E1S8–6	Ceramics and soils impregnated with possible pork fat
	E5T1S-6	Pile hole sediment
	E9T2NE-6A	Dark stain feature, walls
	E9T1NE-6A	Spot 2, dark spot feature
	E2S4–3A	Coal stain
	E4S7–1	Hut
	E10S1–3	Hut
Bitoca 2	E4S5–4	Stake hole
	E4S7–4	Dark stake hole
	E4S1–5	Hole interior

Infrared absorption spectrometry

The vibrational signatures in the infrared region of organic (e.g., C-O or C-C) and inorganic compounds (e.g., P-O in phosphates, C-O in carbonates; Si-O in silicates) present in the samples were recorded in a Bruker FTIR Equinox 55 spectrometer, model IFS66. The samples were pulverized to obtain a fine powder and dispersed in KBr pellets (10 mg sample/300 mg KBr). For each IR spectrum, 256 vacuum atmosphere scans were used with a resolution of 4 cm^{-1}. IR spectra were recorded using 55/S OPUS software.

Scanning electron microscopy (SEM)

The mineralogical characterizations in the TPA samples were complemented by scanning electron microscopy, coupled with energy dispersion (SEM-EDS), which allowed capturing the images and performing micropunctual chemical determinations. The samples were dried at 50°C for 4 h, placed on aluminum platforms, with double-sided carbon adhesive tape and metalized with gold. The electronic backscatter detector allowed the elaboration of chemical concentration distribution maps. The equipment used was a model LEO I450 VP 500 DP microscope and Gresham SED detector, using IXRF software.

Chemical analysis

The TPA samples were air dried and pulverized in agate grade for total chemistry analysis for the elements Ca, P, Zn, Cu, and Mn. The analyzes were performed by ICP-MS, after fusion with $LiBO_2$ and dissolution with aqua regia, performed at the commercial laboratory Geosol LTDA. For analysis of TPI fertility, the methodological procedures are summarized in the Table 2.

14754754, 2024, 6, Downloaded from https://onlinelibrary.wiley.com/doi/10.1111/arcm.12977 by Museu Paraense Emílio Goeldi, Wiley Online Library on [15/01/2025]. See the Terms and Conditions (https://onlinelibrary.wiley.com/terms-and-conditions) on Wiley Online Library for rules of use; OA articles are governed by the applicable Creative Commons License

TABLE 2 Methodologies applied in chemical analysis of soil samples.

Elements	Methods used	Analytical technique	Reference
Dissolved organic matter	Potassium permanganate boiling method	Fluorescence spectroscopy	Liu et al., 2020
Organic matter	Frenkel-Halsey-Hill method	Infrared spectroscopy	Liu et al., 2020
Soil organic matter	Mathematical fractionation approach	Thermogravimetry	Kučerík et al., 2018
Microplastics	Pyrolytic procedure	Thermoanalytical methods	Becker et al., 2020
Heavy metals	Microwave digestion	Inductively coupled plasma—mass spectrometry (ICP-MS),	Choi et al., 2019
Pb^{2+}	Microfluidic paper-based solution sampling	Potentiometry	Ding et al., 2020

RESULTS AND DISCUSSIONS

Mineralogical characterization

Figure 2 shows the X-ray diffractograms of the samples from the Bitoca I and II sites. As can be seen, the samples mostly showed common mineralogy that was composed of kaolinite and quartz, which was well correlated with the mineralogy of Amazonian soils (Costa et al., 2009; da Costa et al., 2011; Huamán et al., 2021; Ishida et al., 2018; Junior et al., 2021). The presence of the amorphous metakaolinite phase was also identified by raising the background between 20 and 30° (2 theta) of the XRD patterns of the samples studied, the formation of which occurs due to the high temperature heating of the kaolinite mineral. Other common mineral phases were identified such as muscovite, anatase, and gibbsite, but in lower quantities. Cristobalite present in most samples (E1S8-6, E2S3-4, E5T1S-6, E6T1N-5, E7T1SE-7, E9T2NE-6, E4S7-4, E4S5-4, E10S1-3) suggested the calcination of amorphous silica, a phase normally found in plants from the region such as cariapé and cauixi (da Costa et al., 2011; Fernandes & Salomão, 2018). It was also observed the peaks due to the presence of calcite ($CaCO_3$) in the samples E3SO-1A4 (sediment with ash and burnt clay from a campfire), E4S5-4 (stake hole), and E10S1-3 (hut), which could be related to shell deposits, also known as sambaquis, or even associated with diet (consumption of shellfish), accumulation of bone remains, or funerary rituals (Klokler et al., 2010). The samples E2S13SO-5, E7T1SE-6, and E10S1-3 were the ones with the highest participation of hematite and goethite, which according to da Costa et al. (2009), the presence of these iron (III) oxyhydroxide minerals may indicate intense organic matter activity in the reduction and degradation of the samples. In addition to being one of the primary soil types seen in the early stages of human settlements, yellow latosol, a form of soil antecedent to TPI, is also one of its principal soil types (Damaceno et al., 2020).

The infrared IR spectra of the samples identified by X-ray diffraction (Bitoca I) were obtained to confirm the phases and are shown in Figure 3. Discussions of the results obtained were divided into three regions as shown below,

All samples showed vibration bands at 3690 ± 10, 3650 ± 10, and 3620 ± 10 cm^{-1} (Figure 3). These bands are related to the Al-O-H stretching vibrations of kaolinite. The band around 3440 ± 10 cm^{-1} (E1S8-6, E5T1S-6, E6T1N-5, and E7T1SE-7), according to Ray et al. (1999) and Beutelspacher and van der Marel (1976), refers to the Al-O-H stretching of the mineral gibbsite. Bands around 3400 cm^{-1} (E3SO-1A4, E2S3-4) refer to the O-H stretches of carboxylic groups and aromatic rings of humic and fulvic acids (Jayaganesh & Senthurpandian, 2010; Qian et al., 2022), as well as C-H aliphatic bonds of these substances

14754754, 2024, 6, Downloaded from https://onlinelibrary.wiley.com/doi/10.1111/arcm.12977 by Museu Paraense Emílio Goeldi, Wiley Online Library on [15/01/2025]. See the Terms and Conditions (https://onlinelibrary.wiley.com/terms-and-conditions) on Wiley Online Library for rules of use; OA articles are governed by the applicable Creative Commons License

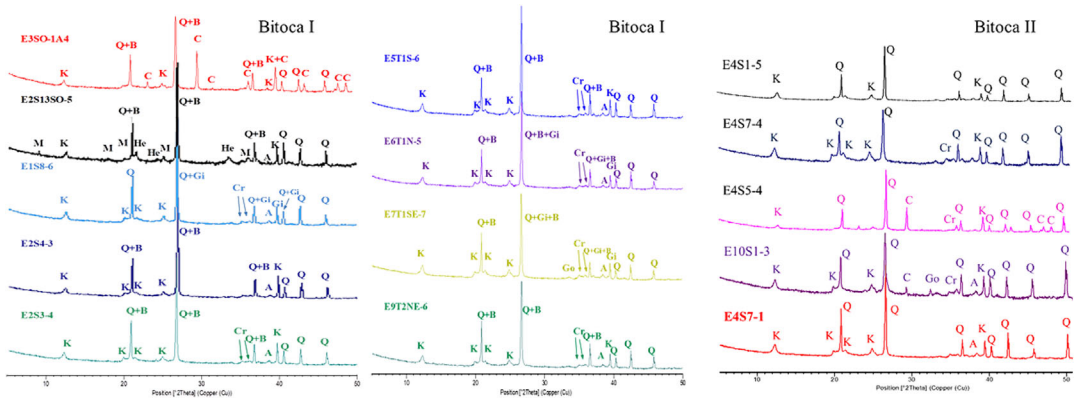

FIGURE 2 X-ray diffraction patterns found in samples from the Bitoca I and II sites. A = anatase, C = calcite, Gb = gibbsite, go = goethite, he = hematite, K = kaolinite, M = muscovite, Q = quartz.

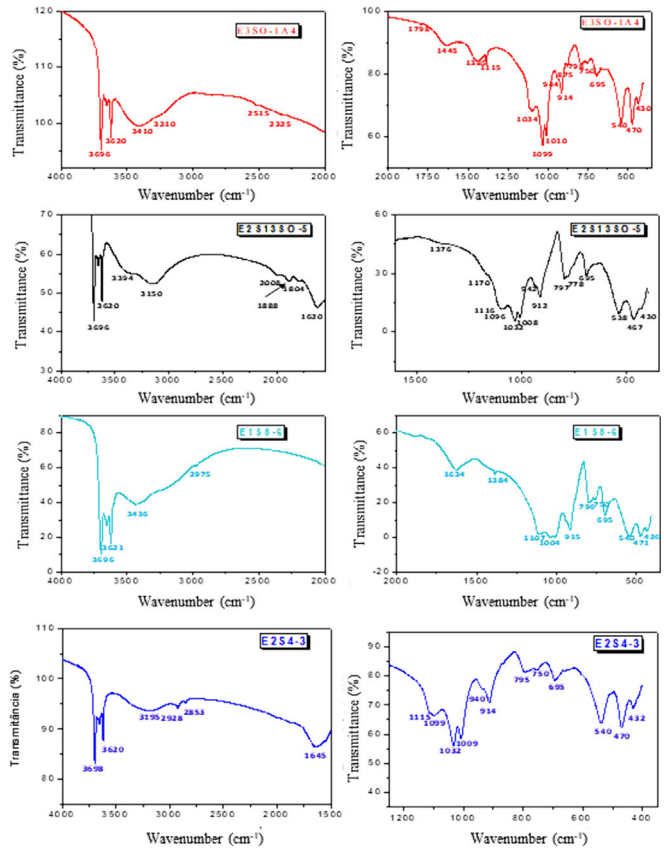

FIGURE 3 Infrared spectra of samples from the Bitoca I site.

around 2922 and 2851 cm^{-1} in samples E2S4-3 and E9T2NE-6 (Beutelspacher & van der Marel, 1976). Calcite CO_3^{2-} stretch bands were observed at 3210, 2515, and 2325 cm^{-1} (Hsiao et al., 2019) in E3SO-1A4.

14754754, 2024, 6, Downloaded from https://onlinelibrary.wiley.com/doi/10.1111/arcm.12977 by Museu Paraense Emilio Goeldi, Wiley Online Library on [15/01/2025]. See the Terms and Conditions (https://onlinelibrary.wiley.com/terms-and-conditions) on Wiley Online Library for rules of use; OA articles are governed by the applicable Creative Commons License

In the 2000–1100 cm^{-1} region of E2S13SO-15, E6T1N-5, E7T1SE-7, and E9T1NE-6 samples exhibited similar bands of O-H groups (1650 and 1630 cm^{-1}) are generally adsorbed on the surface and in the lattice of minerals (kaolinite, goethite, and gibbsite) (Figure 3). The band at 1798 cm^{-1} in sample E3SO-1A4 corresponds to the stretching of the H-O bond of amorphous $CaCO_3$ (Luna Vera et al., 2018), whereas the band at 1445 cm^{-1} relates to the ν_3-CO_3 stretching of crystalline calcite (Devajaran et al., 2007). Stretches of O-H, C-O groups in phenols, and COO– and C-H strains of CH_3 from humic acids were identified at 1385 and 1376 cm^{-1} in almost all samples except E9T2NE-6 (Sakellariadou, 2006). The bands at 1115 and 1030 cm^{-1} observed in samples E2S13SO-5, E2S4-3, E2S3-4, E5T1S-6, and E9T2NE-6 refer to the stretching of tetrahedra of amorphous calcium phosphate groups because they were not identified the presence of phosphate minerals in the sample (Pinzaru & Onac, 2009; Rokita et al., 2000). This inorganic compound may be associated with the presence of bone and cartilage derivatives.

The bands in the 1100–400 cm^{-1} regions corresponded to the metal-oxygen or non-metal-oxygen vibrations of the minerals present. For example, Fe-O vibration bands of goethite and hematite at 695, 539, 471 cm^{-1} (Liu et al., 2021); Si-O stretch bands at 1102, 1033, 796, 471, and 431 cm^{-1} of quartz and kaolinite (Tchakoute et al., 2015); Ti-O vibration bands for anatase at 748 and 540 cm^{-1}. Vibration bands Al-O-H from gibbsite and kaolinite at 939 and 914 cm^{-1} and Si-O-Al from kaolinite at 1010, 752, 695, and 539 cm^{-1} are found (Sadri et al., 2018). A band at 877 cm^{-1} in sample E3SO-1A4 refers to ν_2-CO_3 stretching of calcite from mollusc shells (Loftus et al., 2015). Stretching of the P-O bonds of the PO_4 tetrahedra has also been identified that can be correlated to an amorphous phosphate phase at 940, 700, and 430 cm^{-1} (Kababya et al., 2015; Rokita et al., 2000).

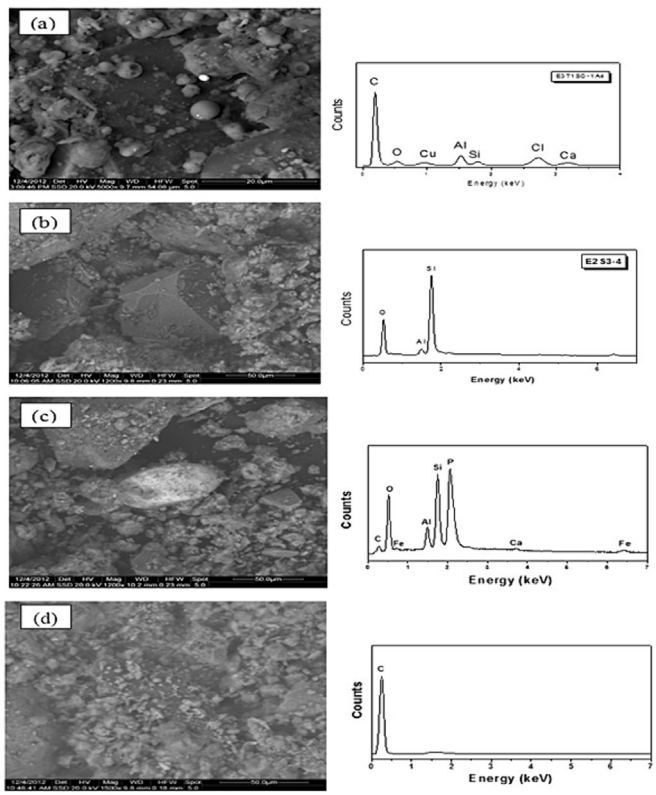

FIGURE 4 Image and semiquantitative chemical analysis obtained by SEM-EDS of samples collected at the Bitoca 1 site: (a) E3SO-1A4; (b) E2S3-4; (c) E6T1N-5; (d) E1S8-6.

14754754, 2024, 6, Downloaded from https://onlinelibrary.wiley.com/doi/10.1111/arcm.12977 by Museu Paraense Emilio Goeldi, Wiley Online Library on [15/01/2025]. See the Terms and Conditions (https://onlinelibrary.wiley.com/terms-and-conditions) on Wiley Online Library for rules of use; OA articles are governed by the applicable Creative Commons License

A morphological investigation of TPI samples from Bitoca 1 was investigated by scanning electron microscopy with spot chemical analysis by EDS (Figure 4).

For sample E3SO-1A4 (Figure 4a), an agglomerate of small spherical particles with an average size of 3–6 μm, was clearly observed. Chemical analysis by EDS revealed the majority presence of carbon, oxygen, and calcium, which suggested the presence of residues of $CaCO_3$-based materials in this sample. Cristobalite crystals with a well-formed tetrahedral habit with a diameter of 70 m were identified in E2S3-4 (Figure 4b), corroborating the X-ray and infrared diffraction data. Bone fragments were visualized in the E6T1N-5 sample (Figure 4c), whereas charcoal micro-aggregates in E1S8-6 (Figure 4d). The Figure 5a (E10-3) showed images of platelets, typical of kaolinite, which is a clay mineral common in tropical regions, especially in the Amazon region. See also the quartz minerals (E4S1-5) in Figure 5b and the anatase mineral (E4S5-4) in Figure 5c. These results corroborated those of XRD.

Chemical characterization of TPI

Figure 6 shows the results of the total chemical composition for Ca and P of the Bitoca I and II samples. Based on the results obtained, the sample E4S7-1 is observed to have the highest levels of Ca (10,460 ppm) and P (1700 ppm). Similar behavior to that observed in sample E10S1-3 showed high levels of Ca (3380 ppm) and P (1500 ppm). Considering that such samples come from hut structures, it is suggested that they were enriched from the day-to-day activities (cooking, disposal of food, animal and vegetable residues, etc.) carried out by prehistoric man (Kämpf & Kern, 2005; Lima et al., 2002). Samples E3SO-1A4, E7T1SE-7, E7T1SE-6, and E6T1N5 (fires) also showed high levels of the macroelements studied, ranging from

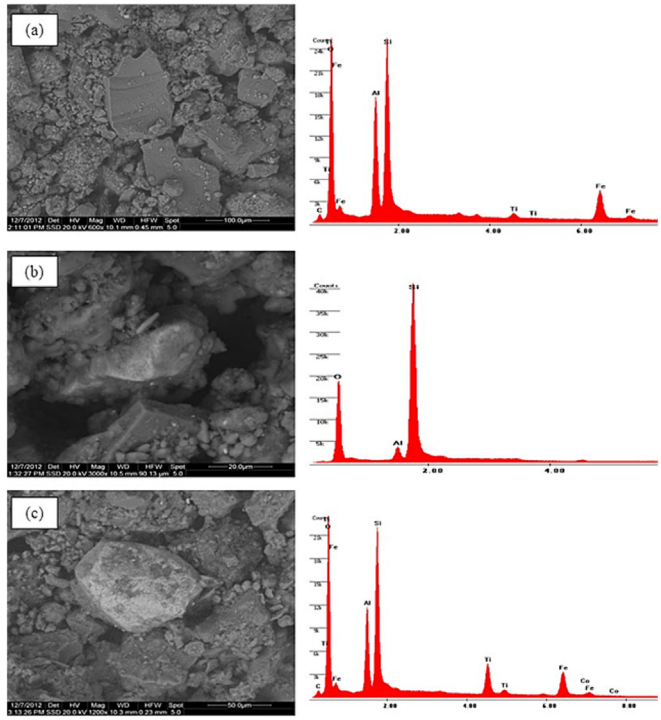

FIGURE 5 Image and semiquantitative chemical analysis obtained by SEM-EDS of samples collected at the Bitoca 2 site: (a) E10-3; (b) E4S1-5; (c) E4S5-4.

14754754, 2024, 6, Downloaded from https://onlinelibrary.wiley.com/doi/10.1111/arcm.12977 by Museu Paraense Emilio Goeldi, Wiley Online Library on [15/01/2025]. See the Terms and Conditions (https://onlinelibrary.wiley.com/terms-and-conditions) on Wiley Online Library for rules of use; OA articles are governed by the applicable Creative Commons License

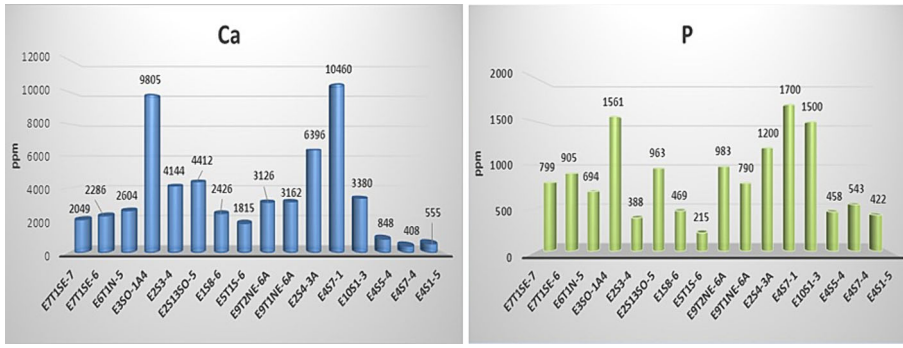

FIGURE 6 Total chemical composition of ca and P of Bitoca I samples (E7T1SE-7; E7T1SE-6; E6T1N-5; E3SO-1A4; E2 S3-4; E2S13SO-15; E1S8-6; E5T1S-6; E9T2NE-6A; E9T1NE-6 e E2S4-3A) e Bitoca II (E4S7-1; E10S1-3; E4S5-4; E4S7-4 e E4S1-5).

9805–2049 ppm for Ca and from 1561–694 ppm for P (Kern et al., 2017; Lehmann, Kern, German, et al., 2003; Macedo et al., 2019; Quesada et al., 2020; Silva & et al., 2021). These bonfires were believed to be used for cooking food (fish, chicken, pork) or even in religious rituals that sacrificed animals.

The values of the microelements (Mn, Cu, and Zn) were also considered high and are shown in Appendix S1. The element Mn showed the highest levels ranging from 1030 to 340 ppm, whereas Zn was in the range of 75 to 26 ppm and Cu between 93 and 48 ppm. In the case of the samples referring to bonfires (E3SO-1A4, E7T1SE-7, E7T1SE-6, and E6T1N5) and huts (E4S7–1 and E10S1–3), the enrichment of these microelements may have been generated from the palm leaves normally used in the construction or burning of these structures (Li et al., 2016).

The characterization of the fertility parameters of TPI soils was carried out and the results are shown in Table 3.

The pH values revealed an average of 5.26 for H_2O and 5.16 for KCl (1 mol. L^{-1}), and are in agreement with the average values of pH observed for TPI found in the Amazon (Falcão & Borges, 2006; Moreira, 2007). Samples EIS8-6 and E6TIN-5 showed the highest negative pH values and, at the same time, presented the highest levels of Al^{3+} (0.91 and 0.89 cmolc/kg). These results indicate a higher content of silicate minerals (Barker et al., 2018), which is in agreement with the results obtained from X-ray diffraction. On the other hand, samples E5T1S-6 and E9T2NE-6 showed higher values of positive pH, which is indicative of the majority presence of the aluminum and iron oxide phases.

The samples referring to sediments collected in a bowl (E9T2NE-6), main hole sediments (E1S8-6 and E2S3-4), and campfire (E3SO-1A4, E7T1SE-7, E7T1SE-6, and E6T1N5) showed the highest levels of organic matter, organic carbon, and nitrogen. As reported by Da Cruz et al. (2022), the higher the organic matter content, the greater the presence of macro and micronutrients in the sample (Liu et al., 2020). The results observed in Table 3 confirm the observations of these authors, because the samples that presented the highest content of organic matter were, in a way, those that also showed high levels of Ca, K, P, Mg, Cu, Zn, and Mn. Regarding the values of exchangeable Ca and available P, high levels were observed in the campfire samples (E6T1N-5 and E7T1SE-7), sediment collected in a bowl (E9T2NE-6), and pile hole sediment (E2S3–4). The relatively high levels of Ca (32.9 cmolc/Kg) and P (374 mg/kg) in E9T2NE-6 suggest that the bowl's function was for cooking or storing food. In bonfires, it may be related to the accumulation of ash, fish bones, or even other animals (Casey & Ludwig, 2018). Regarding the results of SB and CTC of the structures, the values obtained were

14754754, 2024, 6, Downloaded from https://onlinelibrary.wiley.com/doi/10.1111/arcm.12977 by Museu Paraense Emílio Goeldi, Wiley Online Library on [15/01/2025]. See the Terms and Conditions (https://onlinelibrary.wiley.com/terms-and-conditions) on Wiley Online Library for rules of use; OA articles are governed by the applicable Creative Commons License

TABLE 3 Chemical properties of TPI soils from Bitoca I.*.

	pH			C	MO	N			Na	K	Ca	Mg	P	S	CEC	V	Cu	Zn	Mn
Sample	H_2O	KCl	ΔpH	g kg^{-1}			C/N	H + Al	cmolc kg^{-1}				mg kg^{-1}	cmolc kg^{-1}		%	mg kg^{-1}		
E7T1SE-7	5.32	5.18	0.14	13.91	23.99	0.51	27.39	3.80	2.03	2.73	12.63	0.68	34.76	18.06	21.86	82.62	8.19	7.33	243.60
E7T1SE-6	5.38	5.13	0.25	7.42	12.79	0.45	16.43	3.79	1.35	1.36	12.08	0.73	34.76	15.52	19.22	80.75	6.76	3.76	167.01
E7T1N-5	5.07	5.24	−0.21	15.77	27.19	1.02	15.52	9.10	2.03	2.73	25.08	1.10	221.40	30.94	40.04	77.27	6.27	11.97	354.77
E2S3–4	5.82	5.76	0.06	17.63	30.39	1.81	9.76	4.70	2.03	2.73	16.13	1.33	34.56	22.22	26.92	82.54	3.82	11.00	698.48
E1S8–6	4.72	4.93	−0.21	20.41	35.18	1.19	17.22	9.50	1.35	2.05	50.09	0.93	32.62	54.42	63.92	85.14	4.36	7.72	564.29
E5T1S-6	5.41	5.15	0,26	10.20	17.59	1.35	7.53	5.80	2.70	2.73	30.57	1.27	9.59	32.27	42.97	86.73	5.27	1.32	492.21
E9T2NE-6	5.48	5.21	0,27	25.05	43.18	1.07	23.35	4.80	1.35	2.05	22.90	1.21	374.52	27.50	32.30	85.14	5.99	36.51	602.11
E9T1NE-6	4.98	4.90	0,08	14.84	25.59	0.68	21.91	1.90	0.68	1.36	11.29	1.73	209.68	15.06	16.96	88.80	8.06	16.02	512.20
E2S4–3A	5.03	5.08	−0,05	13.91	23.99	1.19	11.74	5.80	2,70	4.09	17.88	0.83	19.04	25.51	31.31	81.48	4.51	5.66	651,14
E4S7–1	5.32	Nd	Nd	8.60	9.40	0.71	12.11	7.20	1.23	2.90	11.90	2.45	22.30	15.30	22.30	67.80	0.95	7.22	200.9
E10S1–3	5.30	Nd	Nd	21.30	4.79	0.42	50.71	7.50	1.25	3.10	7.88	1.35	28.00	9.31	16.91	55.10	2.78	4.20	112.50
E4S5–4	4.61	Nd	Nd	15.58	26.87	1.02	15.34	4.95	1.35	2.05	15.30	0.60	17.77	0.92	15.20	83.10	3.55	5.74	137.98
E4S7–4	4.29	Nd	Nd	12.99	22.39	0.73	17.70	5.40	2.03	2.73	8.02	1.38	11.49	13.97	7.80	41,90	5.59	2.60	103.93
E4S1–5	4.41	Nd	Nd	11.87	20.47	1.07	11.07	6.30	2.70	2.73	1.27	0.62	10.01	9.16	3.31	31.50	5.31	1.12	127.77

Note: *Due to the small amount of mass of samples E3SO-IA4 and E2SOI3S-5, fertility studies were not performed for these samples.
Abbreviations: C, organic carbon; CTC, cation exchange capacity at pH = 7; MO, organic matter; n.d, not determined; SB, sum of bases; V, base saturation.

14754754, 2024, 6, Downloaded from https://onlinelibrary.wiley.com/doi/10.1111/arcm.12977 by Museu Paraense Emilio Goeldi, Wiley Online Library on [15/01/2025]. See the Terms and Conditions (https://onlinelibrary.wiley.com/terms-and-conditions) on Wiley Online Library for rules of use; OA articles are governed by the applicable Creative Commons License

very high, ranging from 18.08–54.42 cmolc/Kg for SB and 21.86–63.92 cmol/Kg for CTC. It stands out among the values obtained from the pile hole sediment samples (E1S8-6 and E5T1S-5) that showed high levels for SB (54.42 and 37.27 cmolc/Kg) and CTC (63.92 and 47.97 cmolc/Kg), which according to studies can be considered as very good (Robinson et al., 2021).

CONCLUSION

The results of the mineralogical and geochemical characterization of the soil samples from the Bitoca I and II sites confirm that they were formed by various human occupation activities by the original peoples of the Amazon and can contribute to the discussion on the fertility of anthrosols (anthropogenic soils) found in the region. The presence of kaolinite with a low degree of crystallinity and metakaolinite (an amorphous phase originating from kaolinite under heating) seems to represent products of weathering or partial burning through activities/rituals carried out on the sites. The identification of calcite and amorphous calcium phosphate shows that the soil was enriched with these inorganic phases as a result of food discards from a diet rich in fish, molluscs and crustaceans, or even rituals. The chemical similarity of the TPA soils at both sites suggests that they were developed through pedogenetic transformation with the introduction of organic and inorganic materials (Ca, P, Mn, Cu, and Zn), also the result of human activity (bones, fruit, and fleshy materials).

ACKNOWLEDGEMENTS

We would like to thank so much Dr. Dirse Kern and Dr. Maura Imazio for their help in the construction of this work. We acknowledge support from Coordination for the Improvement of Higher Education Personnel and National Council for Scientific and Technological Development for scientific support.

PEER REVIEW

The peer review history for this article is available at https://www.webofscience.com/api/gateway/wos/peer-review/10.1111/arcm.12977.

DATA AVAILABILITY STATEMENT

The data employed to support the findings of this research are included within the article.

ORCID

Bruno Apolo Miranda Figueira https://orcid.org/0000-0002-0507-8662

REFERENCES

Athayde, S., & Silva-Lugo, J. (2018). Adaptive strategies to displacement and environmental change among the Kaiabi indigenous people of the Brazilian Amazon. *Society & Natural Resources*, *31*, 666–682. https://doi.org/10.1080/08941920.2018.1426801

Barker, W. W., Welch, S. A., & Banfield, J. F. (2018). Biogeochemical weathering of silicate minerals. In J. F. Banfield & K. H. Nealson (Eds.), *Geomicrobiology* (pp. 391–428). De Gruyter.

Becker, R., Altmann, K., Sommerfeld, T., & Braun, U. (2020). Quantification of microplastics in a freshwater suspended organic matter using different thermoanalytical methods – outcome of an interlaboratory comparison. *Journal of Analytical and Applied Pyrolysis*, *148*, 104829. https://doi.org/10.1016/j.jaap.2020.104829

Beutelspacher, H., & van der Marel, H. W. (1976). *Atlas of infrared spectroscopy of clay minerals and their admixtures*. Elsevier.

Birk, J. J., Teixeira, W. G., Neves, E. G., & Glaser, B. (2011). Faeces deposition on Amazonian Anthrosols as assessed from 5β-stanols. *Journal of Archaeological Science*, *38*, 1209–1220. https://doi.org/10.1016/j.jas.2010.12.015

Casey, W. H., & Ludwig, C. (2018). Silicate mineral dissolution as a ligand-exchange reaction. In A. F. White & S. L. Brantley (Eds.), *Chemical weathering rates of silicate minerals* (pp. 87–118). De Gruyter.

14754754, 2024, 6, Downloaded from https://onlinelibrary.wiley.com/doi/10.1111/arcm.12977 by Museu Paraense Emilio Goeldi, Wiley Online Library on [15/01/2025]. See the Terms and Conditions (https://onlinelibrary.wiley.com/terms-and-conditions) on Wiley Online Library for rules of use; OA articles are governed by the applicable Creative Commons License

Choi, S. H., Kim, J. Y., Choi, E. M., Lee, M. Y., Yang, J. Y., Lee, G. H., Kim, K. S., Yang, J.-S., Russo, R. E., Yoo, J. H., Kang, G.-J., & Park, K. S. (2019). Heavy metal determination by inductively coupled plasma – mass spectrometry (ICP-MS) and direct mercury analysis (DMA) and arsenic mapping by femtosecond (fs) – laser ablation (LA) ICP-MS in cereals. *Analytical Letters*, *52*, 1–14. https://doi.org/10.1080/00032719.2018.1471484

Costa, J. A., Kern, D. C., Costa, M. L., Rodrigues, T. E., Kämpf, N., Lehmann, J., & Frazão, F. J. L. (2009). Geoquímica das terras pretas amazônicas. *As Terras Pretas de Índio da Amazônia: Sua caracterização e Uso Deste Conhecimento na criação de Novas áreas*, *2*, 162–171.

da Costa, M. L., Rios, G. M., Da Silva, M. M. C., Da Silva, G. J., & Molano-Valdes, U. (2011). Mineralogia e química de fragmentos cerâmicos arqueológicos em sítio com Terra Preta da Amazônia Colombiana. *Rem Revista Escola de Minas*, *64*, 17–23. https://doi.org/10.1590/S0370-44672011000100002

Da Cruz, R. S., Ribeiro, J. S., De Moura, L. S., Lopes, R. B., Do Carmo Freitas Faial, K., Gul, K., & Taube, P. S. (2022). Determination of heavy metals by inductively coupled plasma optical emission spectrometry in water samples from Lake Iripixi, Oriximiná, PA, Brazil. *Water, Air, & Soil Pollution*, *233*, 247. https://doi.org/10.1007/s11270-022-05726-2

Damaceno, J. B. D., Da Silva, W. G., Lima, H. N., De Souza Falcão, N. P., De Jesus Padilha, F., Da Costa Junior, A. B., & Tucci, C. A. F. (2020). Physical, chemical, morphological and mineralogical characterization surface and subsurface in hydromorphic and non-hydromorphic soil of the Central Amazon. *Journal of Agricultural Science*, *12*, 245–261. https://doi.org/10.5539/jas.v12n4p245

Devajaran, A., Khadar, M. A., & Chattopadhyay, K. (2007). Effect of ball milling on chemically synthesized nanoparticles of $CaCO_3$. *Materials Science and Engineering A*, *452*, 395–400. https://doi.org/10.1016/j.msea.2006.10.095

Ding, R., Fiedoruk-Pogrebniak, M., Pokrzywnicka, M., Koncki, R., Bobacka, J., & Lisak, G. (2020). Solid reference electrode integrated with paper-based microfluidics for potentiometric ion sensing. *Sensors and Actuators B: Chemical*, *323*, 128680. https://doi.org/10.1016/j.snb.2020.128680

Falcao, N. P. D. S., Clement, C. R., Tsai, S. M., & Comerford, N. B. (2009). Pedology, fertility, and biology of central Amazonian Dark Earths. In W. I. Woods, W. G. Teixeira, J. Lehmann, C. Steiner, A. M. G. A. WinklerPrins, & L. Rebellato (Eds.), *Amazonian dark earths: Wim Sombroek's vision* (pp. 213–228). Springer. https://doi.org/10.1007/978-1-4020-9031-8_11

Falcão, N. P. S., & Borges, L. F. (2006). Efeito da fertilidade de terra preta de índio da Amazônia Central no estado nutricional e na produtividade do mamão hawaí. (*Carica papaya* L.). *Acta Amazônica*, *36*, 401–406. https://doi.org/10.1590/S0044-59672006000400001

Fernandes, L., & Salomão, R. (2018). Preparation and characterization of mullite-alumina structures formed "in situ" from calcined alumina and different grades of synthetic amorphous silica. *Materials Research*, *21*, 1–9. https://doi.org/10.1590/1980-5373-mr-2017-0783

Glaser, B. (2007). Prehistorically modified soils of Central Amazonia: A model for sustainable agriculture in the twenty-first century. *Philosophical Transactions of the Royal Society B*, *362*, 187–196. https://doi.org/10.1098/rstb.2006.1978

Glaser, B., & Birk, J. J. (2012). State of the scientific knowledge on properties and genesis of anthropogenic dark earths in Central Amazonia (terra preta de Índio). *Geochimica et Cosmochimica Acta*, *82*, 39–51. https://doi.org/10.1016/j.gca.2010.11.029

Glaser, B., Guggenberger, G., Zech, W., & Ruivo, M. D. L. (2003). Soil organic matter stability in Amazonian Dark Earths. In J. Lehmann, D. C. Kern, B. Glaser, & W. I. Wodos (Eds.), *Amazonian dark earths* (pp. 141–158). Springer. https://doi.org/10.1007/1-4020-2597-1_12

Hsiao, Y. H., Wang, B., la Plante, E. C., Pignatelli, I., Krishnan, N. M., Le Pape, Y., Neithalath, N., Bauchy, M., & Sant, G. (2019). The effect of irradiation on the atomic structure and chemical durability of calcite and dolomite. *NPJ Materials Degradation*, *3*, 36. https://doi.org/10.1038/s41529-019-0098-x

Huamán, J. C. L., Nicolodelli, G., Senesi, G. S., Montes, C. R., Perruci, N. A. F., Bezzon, V. D. N., & Milori, D. M. B. P. (2021). Characterization and distribution of mineral phases in an Amazonian humiluvic Spodosol profile by XRPD, HR-TEM, SAED and SEM–EDX. *Environmental Earth Sciences*, *80*, 405–415. https://doi.org/10.1007/s12665-021-09697-1

Ishida, D. A., Vieira-Coelho, A. C., Melfi, A. J., Lucas, Y., Camargo, J. P. B., & Montes, C. R. (2018). Influence of pedogenetic processes on the validity of kaolinite crystallinity indices: A case study of an Amazonian Ferralsol-Podzol soil system with white kaolin. *Applied Clay Science*, *162*, 435–442. https://doi.org/10.1016/j.clay.2018.06.025

Jayaganesh, S., & Senthurpandian, V. K. (2010). Extraction and characterization of humic and fulvic acids from latosols under tea cultivation in South India. *Asian Journal of Earth Sciences*, *3*, 130–135. https://doi.org/10.3923/ajes.2010.130.135

Junior, E. S. F. P., De Souza, W. B., & Santana, G. P. (2021). Fracionamento das Formas de Fósforo em Terra Preta de Índio. *Brazilian Applied Science Review*, *5*, 1368–1383. https://doi.org/10.34115/basrv5n3-007

Kababya, S., Gal, A., Kahil, K., Weiner, S., Addadi, L., & Schmidt, A. (2015). Phosphate–water interplay tunes amorphous calcium carbonate metastability: Spontaneous phase separation and crystallization vs stabilization viewed by solid state NMR. *Journal of the American Chemical Society*, *137*, 990–998. https://doi.org/10.1021/ja511869g

Kämpf, N., & Kern, D. C. (2005). O solo como registro da ocupação humana pré-histórica na Amazônia. *Tópicos em ciência do solo*. *Viçosa, MG, Sociedade Brasileira de Ciência Do Solo*, *4*, 277–320.

14754754, 2024, 6, Downloaded from https://onlinelibrary.wiley.com/doi/10.1111/arcm.12977 by Museu Paraense Emílio Goeldi, Wiley Online Library on [15/01/2025]. See the Terms and Conditions (https://onlinelibrary.wiley.com/terms-and-conditions) on Wiley Online Library for rules of use; OA articles are governed by the applicable Creative Commons License

Kämpf, N.; Woods, W.I.; Kern, D.C.; Cunha, T.J.F. Classificação das terras pretas de índio e outros solos antrópicos antigos. (2009) In: Teixeira, W.G., Kern, D. C., Madari, B. E., Lima, H. N., & Woods, W. (Ed). *As Terras Pretas de índio da Amazônia: Sua Caracterização e Uso deste Conhecimento na Criação de Novas Áreas*. Embrapa Amazônia Ocidental, pp. 87–102.

Kern, D. C., et al. (2017). Terras pretas: Approaches to formation processes in a new paradigm. *Geoarchaeology*, *32*, 694–706. https://doi.org/10.1002/gea.21647

Klokler, D., Villagrán, X. S., Giannini, P. C. F., Peixoto, S., & Deblasis, P. (2010). Juntos na Costa: Zooarqueologia e geoarqueologia de sambaquis do litoral sul catarinense. *Revista Do Museu de Arqueologia e Etnologia*, *20*, 53–75. https://doi.org/10.11606/issn.2448-1750.revmae.2010.89910

Kučerík, J., Tokarski, D., Demyan, M. S., Merbach, I., & Siewert, C. (2018). Linking soil organic matter thermal stability with contents of clay, bound water, organic carbon and nitrogen. *Geoderma*, *316*, 38–46. https://doi.org/10.1016/j.geoderma.2017.12.001

Lehmann, J., Kern, D., German, L., Mccann, J., Martins, G., & Moreira, A. (2003). Soil fertility and production potential. 2003. In: Lehmann, Johannes, Kern, Dirse C., Glaser, Bruno, Woods, William I. (Eds.), Amazonian dark earths: Origin, properties, management: Kluwer Academic Publishers, pp. https://doi.org/10.1007/1-4020-2597-1

Lehmann, J., Kern, D. C., Glaser, B., & Woods, W. I. (2003). *Amazonian dark earths. Origin, properties and management*. Kluwer Academic Publishers. https://doi.org/10.1007/1-4020-2597-1

Li, D. Q., Xiao, T., Cao, Z. J., Phoon, K. K., & Zhou, C. B. (2016). Efficient and consistent reliability analysis of soil slope stability using both limit equilibrium analysis and finite element analysis. *Applied Mathematical Modelling*, *40*, 5216–5229. https://doi.org/10.1016/j.apm.2015.11.044

Lima, H. N., Schaefer, C. E., Mello, J. W., Gilkes, R. J., & Ker, J. C. (2002). Pedogenesis and pre-Colombian land use of "Terra Preta Anthrosols"("Indian black earth") of Western Amazonia. *Geoderma*, *110*, 1–17. https://doi.org/10.1016/S0016-7061(02)00141-6

Liu, D., Du, Y., Yu, S., Luo, J., & Duan, H. (2020). Human activities determine quantity and composition of dissolved organic matter in lakes along the Yangtze River. *Water Research*, *168*, 115132. https://doi.org/10.1016/j.watres.2019.115132

Liu, J., Zhu, R., Ma, L., Fu, H., Lin, X., Parker, S. C., & Molinari, M. (2021). Adsorption of phosphate and cadmium on iron (oxyhydr) oxides: A comparative study on ferrihydrite, goethite, and hematite. *Geoderma*, *383*, 114799. https://doi.org/10.1016/j.geoderma.2020.114799

Loftus, E., Rogers, K., & Lee-Thorp, J. (2015). A simple method to establish calcite: Aragonite ratios in archaeological mollusc shells. *Journal of Quaternary Science*, *30*, 731–735. https://doi.org/10.1002/jqs.2819

Luna Vera, F., Guancha Chalapud, M., Castillo Viveros, I., & Vásquez Medina, E. A. (2018). From eggshells to quicklime: Using carbonate cycle as an integrating concept to introduce students to materials analysis by TGA and FTIR. *Journal of Chemical Education*, *95*, 625–630. https://doi.org/10.1021/acs.jchemed.7b00597

Macedo, R. S., et al. (2019). Amazonian dark earths in the fertile floodplains of the Amazon River, Brazil: An example of non-intentional formation of anthropic soils in the Central Amazon region. *Boletim do Museu Paraense Emilio Goeldi. Ciências Humanas*, *14*, 207–227. https://doi.org/10.1590/1981-81222019000100013

Matuk, F. A., Turnhout, E., Fleskens, L., do Amaral, E. F., Haverroth, M., & Behagel, J. H. (2020). Allying knowledge integration and co-production for knowledge legitimacy and usability: The Amazonian SISA policy and the Kaxinawá indigenous people case. *Environmental Science & Policy*, *112*, 1–9. https://doi.org/10.1016/j.envsci.2020.04.018

Moreira, A. (2007). Fertilidade, matéria orgânica e substâncias húmicas em solos antropogênicos da Amazônia Ocidental. *Bragantia*, *66*, 307–315. https://doi.org/10.1590/S0006-87052007000200015

Moutinho, P., Guerra, R., & Azevedo-Ramos, C. (2016). Achieving zero deforestation in the Brazilian Amazon: What is missing? Zero deforestation in the Brazilian Amazon. *Elementa: Science of the Anthropocene*, *4*, 1–11.

Oonk, S., Slomp, C. P., Huisman, H. J., & Vriend, S. P. (2009). Effects of site lithology on geochemical signatures of human occupation in archaeological house plans in the Netherlands. *Journal of Archaeological Science*, *36*, 1215–1228. https://doi.org/10.1016/j.jas.2009.01.010

Pinzaru, S. C., & Onac, B. P. (2009). Raman study of natural berlinite from a geological phosphate deposit. *Vibrational Spectroscopy*, *49*, 97–100. https://doi.org/10.1016/j.vibspec.2008.05.003

Posey, D. A. (2019). Indigenous ecological knowledge and development of the Amazon. In E. F. Moran (Ed.), *The dilemma of Amazonian development* (pp. 225–257). Routledge. https://doi.org/10.4324/9780429310041-12

Qian, G., Xu, L., Li, N., Wang, K., Qu, Y., & Xu, Y. (2022). Enhanced arsenic migration in tailings soil with the addition of humic acid, fulvic acid and thiol-modified humic acid. *Chemosphere*, *286*, 131784. https://doi.org/10.1016/j.chemosphere.2021.131784

Quesada, C. A., et al. (2020). Variations in soil chemical and physical properties explain basin-wide Amazon forest soil carbon concentrations. *Soil*, *6*, 53–88. https://doi.org/10.5194/soil-6-53-2020

Ray, L. F., Kloprogge, J. T., Russel, S. C., & Szetu, J. L. (1999). Vibrational spectroscopy and dehydroxylation of aluminum (Oxo)hydroxides: Gibbsite. *Applied Spectroscopy*, *53*, 423–434. https://doi.org/10.1366/0003702991946884

Robinson, M., Jaimes-Betancourt, C., Elliott, S., Maezumi, S. Y., Hilbert, L., Alves, D., & Iriarte, J. (2021). Anthropogenic soil and settlement organisation in the Bolivian Amazon. *Geoarchaeology*, *36*, 388–403. https://doi.org/10.1002/gea.21839

14754754, 2024, 6, Downloaded from https://onlinelibrary.wiley.com/doi/10.1111/arcm.12977 by Museu Paraense Emílio Goeldi, Wiley Online Library on [15/01/2025]. See the Terms and Conditions (https://onlinelibrary.wiley.com/terms-and-conditions) on Wiley Online Library for rules of use; OA articles are governed by the applicable Creative Commons License

Rokita, M., Handke, M., & Mozgawa, W. (2000). The $AlPO_4$ polymorphs structure in the light of Raman and IR spectroscopy studies. *Journal of Molecular Structure*, *555*, 351–356. https://doi.org/10.1016/S0022-2860(00)00620-7

Ruivo, M. L. P., Amarante, C. B., Oliveira, M. L. S., Muniz, I. C. M., & Santos, D. A. M. (2009). Microbial population and biodiversity in Amazonian dark earth soils. In W. I. Woods, W. G. Teixeira, J. Lehmann, C. Steiner, A. WinklerPrins, & L. Rebellato (Eds.), *Amazonian dark earths: Wim Sombroek's vision* (pp. 351–362). Springer.

Sadri, S., Johnson, B. B., Ruyter-Hooley, M., & Angove, M. J. (2018). The adsorption of nortriptyline on montmorillonite, kaolinite and gibbsite. *Applied Clay Science*, *165*, 64–70. https://doi.org/10.1016/j.clay.2018.08.005

Sakellariadou, F. (2006). Spectroscopic studies of humic acids from subsurface sediment samples collected across the Aegean Sea. *Mediterranean marine. Science*, *7*, 11. https://doi.org/10.12681/mms.166

Schellekens, J., Almeida-Santos, T., Macedo, R. S., Buurman, P., Kuyper, T. W., & Vidal-Torrado, P. (2017). Molecular composition of several soil organic matter fractions from anthropogenic black soils (Terra Preta de Índio) in Amazonia—A pyrolysis-GC/MS study. *Geoderma*, *288*, 154–165. https://doi.org/10.1016/j.geoderma.2016.11.001

Schmidt, M. J., Py-Daniel, A. R., de Paula Moraes, C., Valle, R. B., Caromano, C. F., Texeira, W. G., Barbosa, C. A., Fonseca, J. A., Magalhães, M. P., do Carmo Santos, D. S., & e Silva, R. D. S. (2014). Dark earths and the human built landscape in Amazonia: A widespread pattern of anthrosol formation. *Journal of Archaeological Science*, *42*, 152–165. https://doi.org/10.1016/j.jas.2013.11.002

Silva, F. A. (2009). As atividades econômicas das populações indígenas amazônicas e a formação das terras pretas: O exemplo dos Asurini do Xingu. In W. G. In: Teixeira, D. C. Kern, B. Madari, H. N. Lima, & W. Woods (Eds.), *As Terras Pretas de Índio da Amazônia: Sua Caracterização e Uso deste Conhecimento na Criação de Novas Áreas* (pp. 54–61). Embrapa.

Silva, L. C. R., et al. (2021). A new hypothesis for the origin of Amazonian dark earths. *Nature Communications*, *12*, 127. https://doi.org/10.1038/s41467-020-20184-2

Silveira, M. I., Oliveira, E. R., Kern, D. C., da Costa, M. L., & Rodrigues, S. F. S. (2011). O sítio Jabuti, em Bragança, Pará, no cenário arqueológico do litoral amazônico. *Boletim do Museu Paraense Emílio Goeldi*, *6*, 335–345. https://doi.org/10.1590/S1981-81222011000200006

Silveira, M. I., Rodrigues, M. C. L. F., & Oliveira, E. R. (2009). *Relatório Final do Projeto de Salvamento arqueológico na área do Projeto Salobo—PA. Relatório de pesquisa*. Museu Paraense Emílio Goeldi.

Silveira, M. I., Rodrigues, M. C. L. F., Oliveira, E. R., & Losier, L. M. (2008). Seqüência cronológica de ocupação na Área do Salobo (Pará). *Revista de Arqueologia*, *21*, 61–84. https://doi.org/10.24885/sab.v21i1.240

Taube, P. S., Hansel, F. A., Dos Santos Madureira, L. A., & Teixeira, W. G. (2013). Organic geochemical evaluation of organic acids to assess anthropogenic soil deposits of Central Amazon, Brazil. *Organic Geochemistry*, *58*, 96–106. https://doi.org/10.1016/j.orggeochem.2013.02.004

Tchakoute, H. K., Rüscher, C. H., Djobo, J. Y., Kenne, B. B. D., & Njopwouo, D. (2015). Influence of gibbsite and quartz in kaolin on the properties of metakaolin-based geopolymer cements. *Applied Clay Science*, *107*, 188–194. https://doi.org/10.1016/j.clay.2015.01.023

Tsai, S. M., O'neill, B., Cannavan, F. S., Saito, D., Falcao, N. P. S., Kern, D., Grossman, J., & Thies, J. (2009). The microbial world of Terra Preta. In W. I. Woods, W. G. Teixeira, J. Lehmann, C. Steiner, A. WinklerPrins, & L. Rebellato (Eds.), *Amazonian dark earths: Wim Sombroek's vision* (pp. 299–308). Springer. https://doi.org/10.1007/978-1-4020-9031-8_15

Wells, E. C., Terry, R. E., Parnell, J. J., Hardin, P. J., Jackson, M. W., & Houston, S. D. (2000). Chemical analyzes of ancient anthrosols in residential areas at Piedras Negras, Guatemala. *Journal of Archaeological Science*, *27*, 449–462. https://doi.org/10.1006/jasc.1999.0490

Wilson, C. A., Davidson, D. A., & Cresser, M. S. (2008). Multi-element soil analysis: An assessment of its potential as an aid to archaeological interpretation. *Journal of Archaeological Science*, *35*, 412–424. https://doi.org/10.1016/j.jas.2007.04.006

Woods, W. I., Teixeira, W. G., Lehmann, J., Steiner, C., WinklerPrins, A., & Rebellato, L. (Eds.). (2009). *Amazonian dark earths: Wim Sombroek's vision*. Springer. https://doi.org/10.1007/978-1-4020-9031-8

SUPPORTING INFORMATION

Additional supporting information can be found online in the Supporting Information section at the end of this article.

How to cite this article: Hosn, M. N. A., Figueira, B. A. M., Junior, P. S. T., da Silva, J. F. B. R., Archanjo, B. S., Gul, K., Malik, S., & da Costa, M. L. (2024). Geochemical signature identifying features and archaeological structures in eastern Amazonian Terra Preta sites. *Archaeometry*, *66*(6), 1191–1204. https://doi.org/10.1111/arcm.12977

14754754, 2024, 6, Downloaded from https://onlinelibrary.wiley.com/doi/10.1111/arcm.12977 by Museu Paraense Emílio Goeldi, Wiley Online Library on [15/01/2025]. See the Terms and Conditions (https://onlinelibrary.wiley.com/terms-and-conditions) on Wiley Online Library for rules of use; OA articles are governed by the applicable Creative Commons License